Available online at www.sciencedirect.com
SCIENCE DIRECT®
Journal of Solid State Chemistry 179 (2006) 1898–1903
JOURNAL OF SOLID STATE CHEMISTRY
www.elsevier.com/locate/jssc

Rapid Communication

Crystal structure of the parent misfit-layered cobalt oxide $[Sr_2O_2]_qCoO_2$

T. Nagai[a,*], K. Sakai[b], M. Karppinen[b,1], T. Asaka[a], K. Kimoto[a], A. Yamazaki[c], H. Yamauchi[b], Y. Matsui[a]

[a]*High Voltage Electron Microscopy Station, National Institute for Materials Science, 1-1 Namiki, Tsukuba 305-0044, Japan*
[b]*Materials and Structures Laboratory, Tokyo Institute of Technology, 4259 Nagatsuta, Midori-ku, Yokohama 226-8503, Japan*
[c]*Department of Resources and Environmental Engineering, Waseda University, 3-4-1 Ohkubo, Shinjuku, Tokyo 169-8555, Japan*

Received 7 November 2005; received in revised form 3 February 2006; accepted 16 March 2006
Available online 19 April 2006

Abstract

The crystal structure of our newly discovered Sr–Co–O phase is investigated in detail through high-resolution electron microscopy (HREM) techniques. Electron diffraction (ED) measurement together with energy dispersive X-ray spectroscopy (EDS) analysis show that an ampoule-synthesized sample contains an unknown Sr–Co–O ternary phase with monoclinic symmetry and the cation ratio of Sr/Co = 1. From HREM images a layered structure with a regular stacking of a CdI_2-type CoO_2 sheet and a rock-salt-type Sr_2O_2 double-layered block is observed, which confirms that the phase is the parent of the more complex "misfit-layered (ML)" cobalt oxides of $[M_mA_2O_{m+2}]_qCoO_2$ with the formula of $[Sr_2O_2]_qCoO_2$, i.e. $m = 0$. It is revealed that the misfit parameter q is 0.5, i.e. the two sublattices of the CoO_2 sheet and the Sr_2O_2 block coexist to form a commensurate composite structure. We propose a structural model with monoclinic $P2_1/m$ symmetry, which is supported by simulations of ED patterns and HREM images based on dynamical diffraction theory.

Keywords: Misfit-layered cobalt oxide; Strontium cobalt oxide; Thermoelectric material; Transmission electron microscopy; Electron diffraction; High resolution electron microscopy

1. Introduction

In recent years, layered cobalt oxides have been in the focus of considerable research interest due to their potential applicability as thermoelectric (TE) materials. Significantly large TE power values comparable to those for compound semiconductors such as Bi_2Te_3 were first revealed for the layered cobalt oxide, Na_xCoO_2 [1]. Owing to its appreciable resistance against heat and oxidative conditions, Na_xCoO_2 is expected to turn out beneficial especially in high-temperature applications. The crystal structure of Na_xCoO_2 is regarded as a regular stacking of a hexagonal CdI_2-type CoO_2 sheet and a partially filled Na layer. More recently, the interest was extended to the water-intercalated derivative $Na_{0.35}CoO_2 \cdot 1.3H_2O$ showing superconductivity [2] and the so-called misfit-layered (ML) cobalt oxides, in which the hexagonal CoO_2 sheet with triangular arrangement of the constituent atoms is coupled incoherently with a rock-salt-type $[(MO)_m(AO)_2]$ block being composed of two types of square-planar planes, MO (M = Co, Bi, Pb, Tl, etc.) and AO (A = Ca, Sr, Ba, etc.), with the layer sequence of AO–$(MO)_m$–AO–CoO_2 [3–14]. With the use of a "misfit parameter" q, the formula can be described as $[M_mA_2O_{m+2}]_qCoO_2$ (the value of q ranges approximately from 0.50 to 0.62 for the known oxides).

Parallel to the case of the Na_xCoO_2 phase, also the ML cobalt oxides exhibit excellent TE characteristics that originate from their layered crystal structures. A large TE power and a high electrical conductivity are given by spin and orbital degrees of freedom which are inherent to the strongly correlated electrons of the CoO_2 sheets. In addition, the insulating rock-salt-type blocks play a role of suppressing the thermal conductivity [15]. The TE

*Corresponding author. Fax: +81 29 860 4700.
E-mail address: NAGAI.Takuro@nims.go.jp (T. Nagai).
[1]New address: Laboratory of Inorganic and Analytical Chemistry, Helsinki University of Technology, FI-02150 Espoo, Finland.

0022-4596/$ - see front matter © 2006 Elsevier Inc. All rights reserved.
doi:10.1016/j.jssc.2006.03.016

performance is controlled by the number and composition of the layers in the rock-salt block, with the value of the misfit parameter q consequently determined. Hence, depending on the choices for m, M and A in $[(MO)_m(AO)_2]$, we may-in principle-achieve materials with different carrier concentrations, thermal conductivities, heat and oxidation resistances, etc. In terms of the parameter "m", the only choices seemed to be 1 and 2, as long as the phases known were concerned. However, very recently, we successfully synthesized the first "$m = 0$" phase with the formula of $[Sr_2O_2]_qCoO_2$ [16]. The new phase with no MO planes can be regarded as the parent of the more complex ML cobalt oxides. Here, we report the detailed process of its structural characterization by means of a comprehensive set of high-resolution electron microscopy (HREM) techniques.

2. Experimental

The Sr–Co–O samples were synthesized in evacuated and sealed quartz ampoules at 850 °C from a mixture of SrO_2 and Co_3O_4 powders with the ratio of 1:1 for Sr and Co [16]. X-ray powder diffraction (XRD) patterns were collected for the samples at room temperature using a Rigaku RINT-2500V diffractometer equipped with a rotating Cu anode. The electron diffraction (ED) patterns and HREM images were obtained using an ultra-high-voltage transmission electron microscope (TEM) Hitachi H-1500 operated at an accelerating voltage of 820 kV. The TEM specimens were prepared by two techniques, i.e. (i) crushing and (ii) ion milling. In (i), the sample is crushed with a mortar into fine fragments, which are ultrasonically dispersed in CCl_4 and transferred to carbon microgrids. In (ii), a mechanically thinned and ground sample is milled by Ar^+ ions with an energy of 4 keV in cooling condition using GATAN-NISSEI 600N DuoMill. The local chemical compositions were determined by energy dispersive X-ray spectroscopy (EDS) analyzer Kevex Sigma attached to a field-emission analytical TEM Hitachi HF-3000S operated at an accelerating voltage of 300 kV. Simulations of ED patterns and HREM images based on dynamical diffraction theory were carried out using the software MacTempas.

3. Results and discussion

The phase composition of the synthesized samples was investigated by XRD measurements. The XRD patterns revealed that besides small amounts of Co_3O_4 and $SrCO_3$ as impurity phases the samples contain an unknown phase (essentially different from the phases such as the spinel Co_3O_4, the brownmillerite $Sr_2Co_2O_5$ and the perovskite $SrCoO_{3-\delta}$ commonly forming in the Sr–Co–O system) with the longest d value of ~9.1 Å [16]. Since our ampoule synthesis produces moderately oxidizing conditions, it appears that the new phase is stabilized within an oxygen-pressure range intermediate between those required to obtain the ambient-pressure-stabilized $Sr_2Co_2O_5$ [17] brownmillerite and the high-oxygen-pressure-synthesized $SrCoO_{3-\delta}$ [18] perovskite. From the XRD data only, it was not possible to extract the lattice parameters and the crystal symmetry of the new phase. Therefore, we employed selected-area ED measurements together with EDS analysis carried out using an analytical TEM. Fig. 1 shows a representative ED pattern taken from a selected area for which the Sr/Co ratio was found to be ~1. The same pattern and cation-ratio combination could be repeatedly verified for a specimen prepared by the crushing method. Most likely the pattern corresponds to a main cross section of the reciprocal lattice of our new Sr–Co–O phase for which Sr/Co ≈ 1. However, for the crushed specimen we observed no patterns showing the d spacing of ~9.1 Å. This implies that cracks easily occur along a specific plane in the crystal of the new phase. To avoid such cleavage we prepared another specimen by the Ar^+-ion milling method. In Figs. 2(a)–(c), we display a set of ED patterns which were observed for the specimen and show the d spacing of ~9.1 Å. The Sr/Co ratio for the selected areas was commonly ~1. Information from the four patterns in Figs. 1 and 2(a)–(c) converges to a possible reciprocal-space unit cell with the parameters, $a^* \approx 0.20\,Å^{-1}$, $b^* \approx 0.18\,Å^{-1}$, $c^* \approx 0.11\,Å^{-1}$, $\alpha^* \approx 90°$, $\beta^* \approx 84°$, and $\gamma^* \approx 90°$. The cell corresponds to a real-space unit cell with the parameters, $a \approx 5.0$ Å, $b \approx 5.6$ Å, $c \approx 9.1$ Å, $\alpha \approx 90°$, $\beta \approx 96°$, and $\gamma \approx 90°$. In the figures the indices are given within a monoclinic cell setting. The direction of electron beam is [001], [010], [−100], and [−110] zone axis for Fig. 1 and Figs. 2(a)–(c), respectively. The $h\,0\,0$ (h = odd) and $0\,k\,0$ (k = odd) reflections are invisible in the [010] and [−100] patterns but clearly visible in the [001] one, indicating that the reflections are induced by multiple scattering of electron

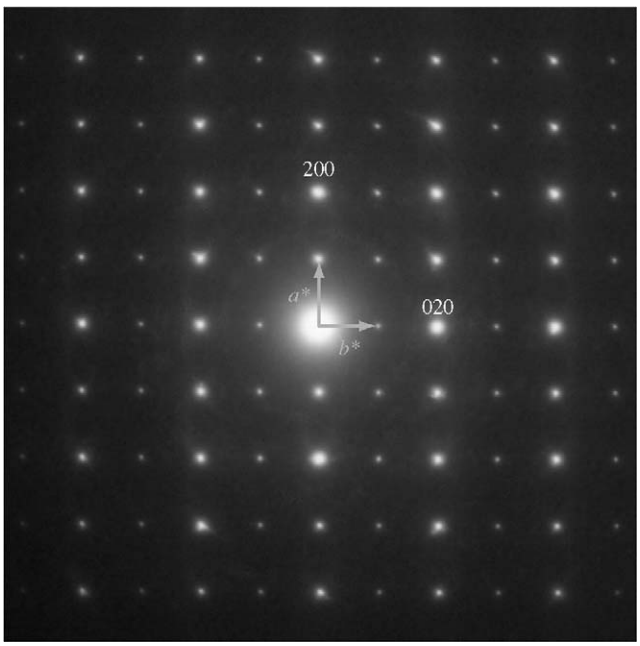

Fig. 1. An ED pattern observed for our new Sr–Co–O phase with Sr/Co ≈ 1. The spots are indexed in the monoclinic cell setting described in the latter part of the text. The direction of electron beam is [001] zone axis.

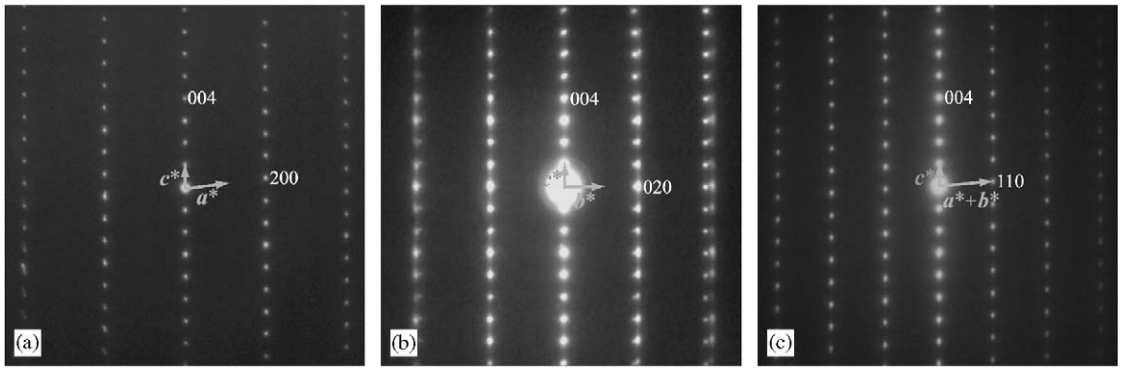

Fig. 2. A set of ED patterns for the Sr–Co–O phase, showing a d spacing of ~9.1 Å. The spots are indexed in the monoclinic cell setting and the directions of electron beam are: (a) [010], (b) [−100], and (c) [−110] zone axes.

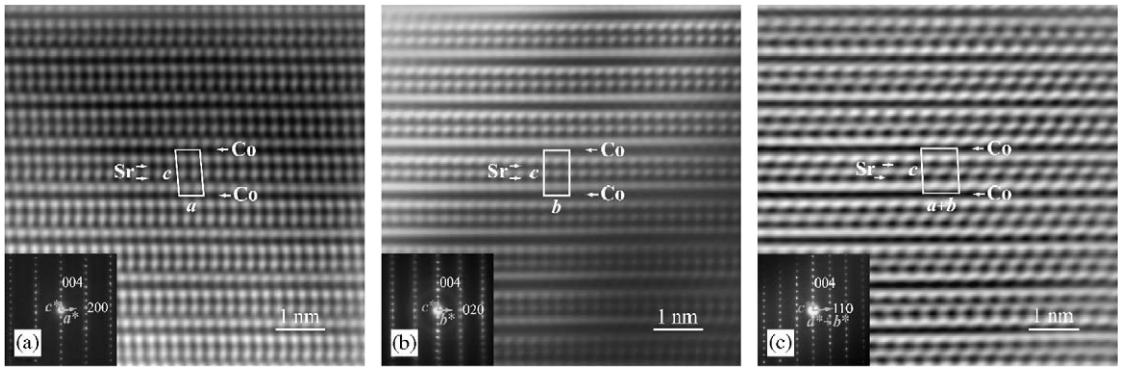

Fig. 3. HREM images and the corresponding ED patterns for the Sr–Co–O phase projected along (a) [010], (b) [−100], and (c) [−110]. The unit cell is indicated by white lines and a–c represent the three-dimensional vectors.

beam in the [001] projection. The X-ray diffraction maxima assigned to the new phase were successfully indexed according to the aforementioned unit cell. The X-ray diffraction pattern with peak indexing was given in our original paper [16]. The precise lattice constants as refined from the XRD data are: $a = 4.980(0.1)$ Å, $b = 5.596(0.1)$ Å, $c = 9.107(0.1)$ Å, and $\beta = 96.28(0.1)^\circ$. The EDS analyses for a large number of specimen areas showed that the average value of the Sr/Co ratio is 0.99(5).

Hence, we were able to successfully reveal the lattice parameters and the chemical composition for our new Sr–Co–O phase. Additional information, highly valuable for the structural determination, was obtained from the HREM observation. The HREM images projected along [010], [−100], and [−110] are shown in Figs. 3(a)–(c), respectively. These images clearly exhibit a layered structure different from perovskite-based structures. Since the images were taken in the vicinity of Scherzer's focus [19], the positions of black dots should correspond to those of cations, i.e. Sr or Co ions. In each image the unit cell is indicated by white lines. It is seen that the layers are stacked along the c-axis. Here, we follow the most plausible assumption and assign the phase as a member of the ML cobalt-oxide family. Among the previously known ML cobalt oxides, $[Ca_2CoO_3]_qCoO_2$ ($q = 0.62$) and $[Sr_2CoO_3]_qCoO_2$ ($q = 0.56$) [7–10] are ternary phases. In the Sr–Co–O phase $[Sr_2CoO_3]_qCoO_2$, the hexagonal CdI_2-type CoO_2 sheet is coupled incommensurately with a $[Sr_2CoO_3]$ block of rock-salt type along the layer sequence of SrO–CoO–SrO–CoO_2. We propose an ML structure for our new Sr–Co–O phase on the basis of the ML structure with the four layers in the unit cell. Because the unit cell of our Sr–Co–O phase according to the HREM images contains three layers, it is necessary to subtract one layer from the "SrO–CoO–SrO–CoO_2" layers to make it consistent with the HREM data. The subtracted layer cannot be CoO_2 or SrO, as these subtractions would both end up with a Sr/Co ratio far from ~1. On the other hand, if we remove the CoO layer in the rock-salt-type block, the formula would be $[Sr_2O_2]_qCoO_2$, which satisfies the condition $Sr/Co \approx 1$ at $q = 0.5$. This structure would also perfectly explain the observed contrasts in the HREM images. The assignments of the ions in the HREM images of Figs. 3(a)–(c) are made on the basis of the "$[Sr_2O_2]_qCoO_2$" structure. The positions of the black dots indicated by "Sr" in each image are consistent with those of Sr ions constituting a rock-salt-type Sr_2O_2 block in the view along the in-plane Sr–O or Sr–Sr direction. It moreover seems that the black layers indicated by "Co" change with the direction of projection in such a way as expected for Co ions in triangular arrangement. Furthermore, the value of misfit parameter $q = 0.5$ well explains the [001] zone-axis ED pattern in

Fig. 1. Fig. 4 illustrates that a [001] zone-axis ED pattern for $[Sr_2O_2]_{0.5}CoO_2$ should exhibit a CoO_2-derived hexagonal (H) reciprocal lattice and a Sr_2O_2-derived square (S) reciprocal lattice which are commensurate with $b_H^*/b_S^* = 2.0$, i.e. $b_H/b_S = q = 0.5$. It is deduced that additional reflections are dynamically induced, namely, multiple reflections occur due to the combination of the two sublattices, resulting in the appearance of the pattern.

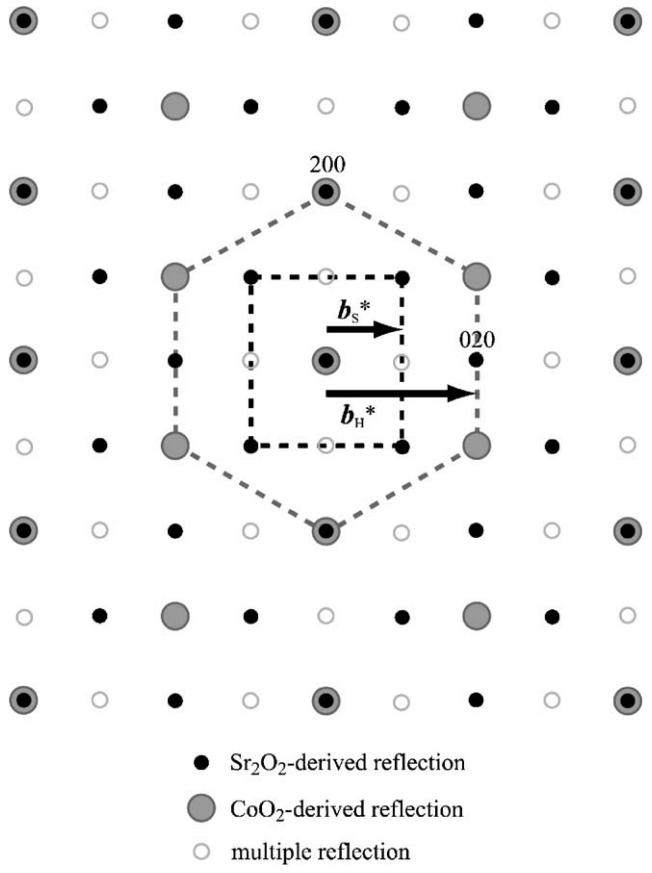

Fig. 4. An illustration of the [001] zone-axis ED pattern for the Sr–Co–O phase. A CoO_2-derived hexagonal (H) reciprocal lattice and a Sr_2O_2-derived square (S) reciprocal lattice are commensurate with $b_H^*/b_S^* = 2.0$. Multiple reflections occur due to the combination of the two sublattices.

On the basis of the ED and HREM results, we constructed a structural model that corresponds to the formula of $[Sr_2O_2]_qCoO_2$ ($q = 0.5$). The model is schematically illustrated by Figs. 5(a)–(c). The crystal structure has monoclinic $P2_1/m$ (no. 11) symmetry and the aforementioned (refined) lattice parameters. The positional parameters are given in Table 1. The oxygen ions of CoO_2 sheets are positioned such that the bonding distances between them and the neighboring Sr ions get reasonable values. The hexagonal CoO_2 sheet is coupled commensurately with the double-layered rock-salt-type Sr_2O_2 block with $b_H/b_S = 0.5$. Simulations based on dynamical diffraction theory and our structural model well reproduced the experimentally observed ED patterns. In particular, the simulated [001] zone-axis pattern is in good agreement with the experimental one. It was also confirmed that with increasing thickness of the specimen (t), the intensities of the multiple reflections increase. Fig. 6(a) shows the [001]

Table 1
Positional parameters of our structural model for $[Sr_2O_2]_qCoO_2$ ($q = 0.5$): space group $P2_1/m$ (no. 11) 2nd setting, $a = 4.980$ Å, $b = 5.596$ Å, $c = 9.107$ Å, and $\beta = 96.28°$

Atom	Site	x	y	z
Co(1)	2*e*	0	0.25	0
Co(2)	2*b*	0.5	0.5	0
Sr(1)	2*e*	−0.02	0.25	0.35
Sr(2)	2*e*	0.48	0.75	0.35
O(1)	2*e*	−0.333	0.25	0.12
O(2)	2*e*	−0.333	0.75	0.12
O(3)	4*f*	0.167	0.5	0.12
O(4)	2*e*	−0.02	0.75	0.37
O(5)	2*e*	0.48	0.25	0.37

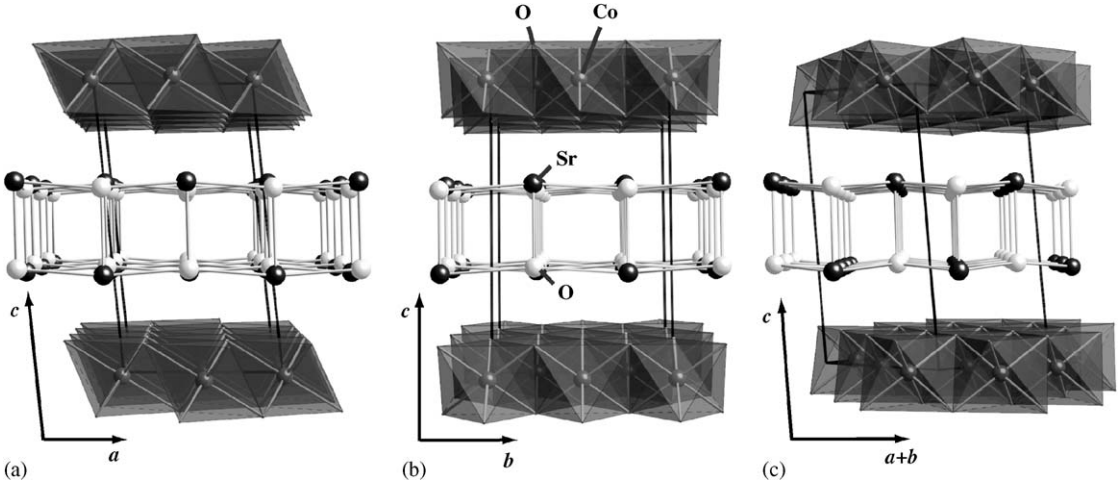

Fig. 5. A crystal structure model proposed for $[Sr_2O_2]_qCoO_2$ ($q = 0.5$) with monoclinic $P2_1/m$ (no. 11) symmetry and lattice parameters, $a = 4.980$ Å, $b = 5.596$ Å, $c = 9.107$ Å, and $\beta = 96.28°$. The directions of the view are: (a) [010], (b) [−100], and (c) [−110].

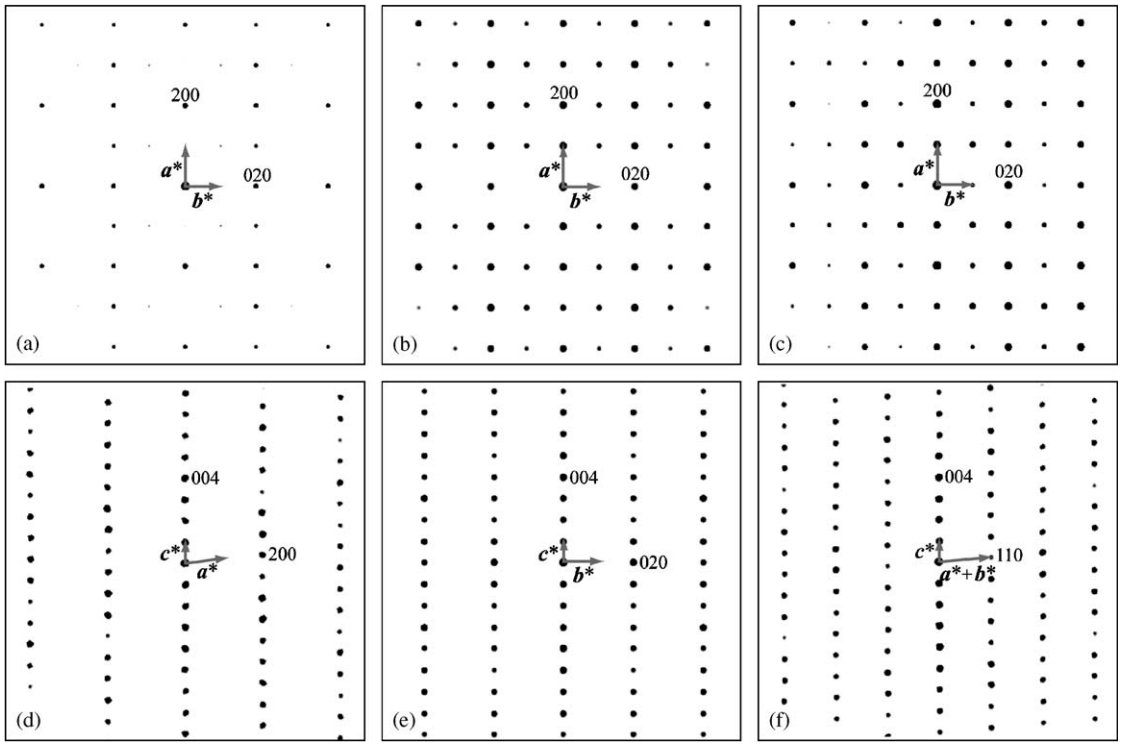

Fig. 6. Simulated [001] zone-axis ED patterns using the model described in Fig. 5 and Table 1. The conditions are: (a) crystal thickness, $t = 10$ Å, and crystal tilt, $h = k = 0$ mrad, (b) $t = 200$ Å and $h = k = 0$ mrad, (c) $t = 200$ Å and $h = k = 10$ mrad. Simulated ED patterns with (d) [010], (e) [−100], and (f) [−110] projections under $t = 200$ Å and $h = k = 0$ mrad.

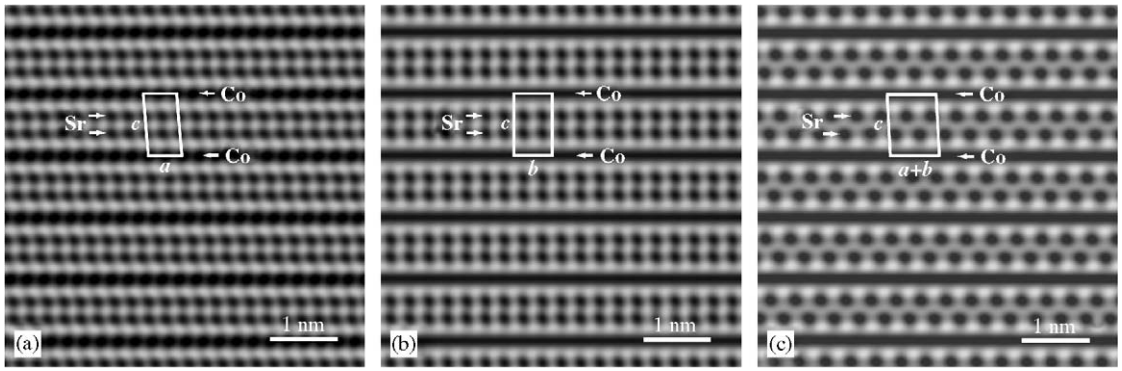

Fig. 7. Simulated HREM images with (a) [010], (b) [−100], and (c) [−110] projections under crystal thickness, $t = 20$ Å and defocus, $\Delta f = -570$ Å (Scherzer's focus).

zone-axis pattern by simulation under the condition that the crystal is very thin, here $t = 10$ Å. As the dynamical effect is less significant for such a case, we should observe only few multiple reflections in the simulated pattern. Actually, the reflections in the pattern are almost consistent with the CoO_2-derived and the Sr_2O_2-derived reflections in the illustration in Fig. 4. For comparison, Fig. 6(b) shows the simulated pattern in the case of a thick crystal, here $t = 200$ Å. A number of multiple reflections appear there as expected. Further, if we assume a crystal tilt of $h = k = 10$ mrad, reflections appear at $(0, 2n+1, 0)$ as shown in Fig. 6(c); the simulated pattern is perfectly consistent with the experimental one in terms of the appearance of reflections. Since simulations show that the $0\,k\,0$ reflections never appear with no crystal tilt, we speculate that the reason for the appearance of these reflections in the [001] zone-axis patterns such as that in Fig. 1 is that local crystal areas have slight deviations from the exact [001] zone-axis orientation. The simulated ED patterns with [010], [−100], and [−110] projections under $t = 200$ Å are shown in Figs. 6(d)–(f), respectively. These patterns too agree with the experimental ones. The simulations also well reproduced the experimental HREM images. The simulated HREM images with [010], [−100], and [−110] projections under defocus, $\Delta f = -570$ Å (Scherzer's focus) are shown in Figs. 7(a)–(c), respectively. These images confirm that the black dots in the experimental images correspond to Sr and Co ions in the

proposed parent or "$m = 0$" ML structure. More recently, a similar "$m = 0$" ML compound with the composition of $(CaOH)_{1.14}CoO_2$ has been reported [20].

The commensurate coupling in the $[Sr_2O_2]_qCoO_2$ ($q = 0.5$) structure is apparently allowed by the large Sr_2O_2 square lattice, which is considerably expanded as compared with the other known Sr-based ML cobalt oxides. A similar coupling with $q = 0.5$ has been observed for the Ba-based ML cobalt oxide, $[Bi_2Ba_{1.8}Co_{0.2}O_4]_{0.5}CoO_2$ [14], whereas only incommensurate couplings with $q > 0.5$ have been confirmed for the other Sr or Ca-based ML compounds. The Ba-based phase has a large rock-salt lattice, which is attributed to the large size of the Ba ions. As for the present Sr-based $m = 0$ phase, we suggest that the expansion of the Sr_2O_2 lattice is caused by the presence of oxygen vacancies [16]. We believe that the valence of cobalt in our new $[Sr_2O_2]_{0.5}CoO_2$ phase is considerably lower than the value of $+4$ that it would be without the oxygen vacancies, since the synthesis conditions are very similar to those employed for other cobalt oxides with the Co valence well below $+3.5$ [21–23]. This assumption is also consistent with the TE power data for the phase showing that the Seebeck coefficient is positive (at temperatures above ~40 K) [16]. Since diffuse reflections with anisotropic shapes, or additional superlattice spots are not seen in the ED patterns, the oxygen vacancies are estimated to randomly exist in O(4) and O(5) sites in the Sr_2O_2 blocks. Our original paper reporting the discovery of the new phase also describes its characterization for the basic physical properties [16]: it was found that this simplest ML phase yet exhibits transport-property characteristics comparable to those of its earlier-established and more complex derivatives.

In conclusion, we have successfully derived the crystal structure of our newly synthesized Sr–Co–O compound, $[Sr_2O_2]_qCoO_2$, through systematic HREM investigation. The structure of the thus verified parent ML phase consists of an alternate stacking of hexagonal CoO_2 sheets and double-layered rock-salt-type Sr_2O_2 blocks, which are commensurately coupled with $q = b_H/b_S = 0.5$. We propose a structural model with monoclinic $P2_1/m$ symmetry, which is supported by simulations of ED patterns and HREM images.

Acknowledgments

We thank M. Owada and C. Tsuruta for specimen preparations and discussions. This work was supported by the Nanotechnology Support Project of the MEXT, Japan, and also by Grants-in-aid for Scientific Research (Nos. 15206002 and 15206071) from the Japan Society for the Promotion of Science. M.K. acknowledges the financial support from the Academy of Finland (Decision No. 110433).

References

[1] I. Terasaki, Y. Sasago, K. Uchinokura, Phys. Rev. B 56 (1997) R12685.
[2] K. Takada, H. Sakurai, E. Takayama-Muromachi, F. Izumi, R.A. Dilanian, T. Sasaki, Nature 422 (2003) 53.
[3] P. Boullay, B. Domenges, M. Hervieu, D. Groult, B. Raveau, Chem. Mater. 8 (1996) 1482.
[4] P. Boullay, R. Seshadri, F. Studer, M. Hervieu, D. Groult, B. Raveau, Chem. Mater. 10 (1998) 92.
[5] M. Hervieu, Ph. Boullay, C. Michel, A. Maignan, B. Raveau, J. Solid State Chem. 142 (1999) 305.
[6] H. Leligny, D. Grebille, O. Pérez, A.C. Masset, M. Hervieu, B. Raveau, Acta Crystallogr. B 56 (2000) 173.
[7] A.C. Masset, C. Michel, A. Maignan, M. Hervieu, O. Toulemonde, F. Studer, B. Raveau, J. Hejtmanek, Phys. Rev. B 62 (2000) 166.
[8] Y. Miyazaki, K. Kudo, M. Akoshima, Y. Ono, Y. Koike, T. Kajitani, Jpn. J. Appl. Phys. 39 (2000) L531.
[9] Y. Miyazaki, M. Onoda, T. Oku, M. Kikuchi, Y. Ishii, Y. Ono, Y. Morii, T. Kajitani, J. Phys. Soc. Jpn. 71 (2002) 491.
[10] D. Pelloquin, S. Hebert, A. Maignan, B. Raveau, Solid State Sci. 6 (2004) 167.
[11] Y. Miyazaki, T. Miura, Y. Ono, T. Kajitani, Jpn. J. Appl. Phys. 41 (2002) L849.
[12] D. Pelloquin, A. Maignan, S. Hébert, C. Martin, M. Hervieu, C. Michel, L.B. Wang, B. Raveau, Chem. Mater. 14 (2002) 3100.
[13] A. Maignan, S. Hébert, M. Hervieu, C. Michel, D. Pelloquin, D. Khomskii, J. Phys. Condens. Matter 15 (2003) 2711.
[14] M. Hervieu, A. Maignan, C. Michel, V. Hardy, N. Creon, B. Raveau, Phys. Rev. B 67 (2003) 045112.
[15] I. Terasaki, J. Crystallogr. Soc. Jpn. 46 (2004) 27.
[16] H. Yamauchi, K. Sakai, T. Nagai, Y. Matsui, M. Karppinen, Chem. Mater. 18 (2006) 155.
[17] T. Takeda, Y. Yamaguchi, H. Watanabe, J. Phys. Soc. Jpn. 33 (1972) 970.
[18] S. Kawasaki, M. Takano, Y. Takeda, J. Solid State Chem. 121 (1996) 174.
[19] O. Scherzer, J. Appl. Phys. 20 (1949) 20.
[20] M. Shizuya, M. Isobe, Y. Baba, T. Nagai, M. Osada, K. Kosuda, S. Takenouchi, Y. Matsui, E. Takayama-Muromachi, cond-mat/0510031.
[21] M. Karppinen, H. Fjellvåg, T. Konno, Y. Morita, T. Motohashi, H. Yamauchi, Chem. Mater. 16 (2004) 2790.
[22] Y. Morita, J. Poulsen, K. Sakai, T. Motohashi, T. Fujii, I. Terasaki, H. Yamauchi, M. Karppinen, J. Solid State Chem. 177 (2004) 3150.
[23] M. Karppinen, I. Asako, T. Motohashi, H. Yamauchi, Phys. Rev. B 71 (2005) 92105.